Journal of Environmental Chemical Engineering 13 (2025) 116047

Contents lists available at ScienceDirect

Journal of Environmental Chemical Engineering

journal homepage: www.elsevier.com/locate/jece

3D printed structured catalyst supports for enhanced CO_2 methanation

Elif Kabakci [a,b,1], Natalia Kostretsova [a,1], Elena Martín Morales [a], Jesús Diaz-Ruiz [a], Albert Tarancón [a,c], Jordi Guilera [a,d], Marc Torrell [a,*]

[a] Catalonia Institute for Energy Research (IREC), Barcelona 08930, Spain
[b] Department of Materials Science and Engineering, Canakkale Onsekiz Mart University, Canakkale, 17100, Türkiye
[c] Institució Catalana de Recerca i Estudis Avançats (ICREA), Barcelona 08010, Spain
[d] Facultat de Química, Universitat de Barcelona, Barcelona 08028, Spain

ARTICLE INFO

Keywords:
3D printing
CO_2 methanation
Catalyst design
Catalytic monoliths

ABSTRACT

This work presents the implementation of ceramic stereolithography 3D printing to generate catalytic supports to investigate the influence of the structured reactor design on its conversion efficiency for CO_2 methanation. Alumina monolithic supports were fabricated by stereolithography using a non-linear channel geometry formed by an array of twisted elements, which was compared to the conventional monolith design. The catalytic performance of the 3D printed monoliths, functionalized with Ni as a catalyst material, was evaluated and complemented by CFD simulation, showing the strong correlation between the support design selection and CO_2 conversion rates. A maximum CO_2 conversion of 84 % at 400 °C was achieved owing to the three-dimensional monolith design, which increased the catalytic activity of the system under high gas flow rates by creating a non-uniform reactant flow distribution with higher turbulence kinetic energy. Therefore, this work demonstrates the potential of ceramic 3D printing technologies to boost the catalytic device efficiency by implementing novel designs, not reproducible by conventional ceramic manufacturing approaches.

1. Introduction

Given the growing environmental concerns and the urgent necessity to prevent climate change, the development of innovative solutions for sustainable energy management is becoming essential. In this context, power-to-gas (PtG) processes offer a promising method for chemical energy storage, based on the reduction of carbon dioxide emissions by their use as a feedstock to produce synthetic fuels. Typically, the process starts with generation of green hydrogen through water/steam electrolysis, which is followed by the catalytic reaction of the produced hydrogen with captured carbon dioxide to be converted to synthetic hydrocarbons. One of the prospective applications of this process is CO_2 methanation, described by Sabatier reaction (1), where green hydrogen is used to obtain a synthetic natural gas (SNG), primarily consisting of methane with residual hydrogen and CO_2 content [1]. The performance of catalytic reactors is highly influenced by process conditions such as temperature, pressure, volume and ratio of the reactants, as well as residence time and flow regime [2]. Typically, catalytic methanation devices operate within temperature range of 200 – 550°C and at pressures ranging from 5 to 25 bars [3]. Although CO_2 methanation is the thermodynamically favored process, it requires the presence of catalyst materials, to overcome the kinetic barrier and reach high conversion levels [1,3].

$$CO_{2(g)} + 4H_{2(g)} \rightleftharpoons CH_{4(g)} + 2H_2O_{(g)} \quad \Delta H^{\circ}_{298K} = -165 kJ \cdot mol^{-1} \qquad (1)$$

CO_2 methanation is sensitive to the structure of the catalyst and its preparation methods [4,5]. The efficiency of the process could be significantly affected by the selection of the catalyst material and the design of the reaction system. Currently, nickel-based catalysts are widely applied for CO_2 methanation due to their high activity, selectivity, and cost-effectiveness [2,6]. In addition to selecting the appropriate catalyst material, a practical challenge in the reactor design is related to the heat distribution management during system operation, which is highly affected by the exothermic nature of the methanation process leading to a generation of hot spots or quenching the reaction [3]. To address these issues and maximize the CO_2 conversion rates, the design of structured catalysts was developed as an alternative for other types of standard reactor configurations, such as fixed-bed systems filled

* Correspondence to: Catalonia Institute for Energy Research (IREC), Jardins de les Dones de Negre 1, 2ª pl., 08930, Sant Adrià del Besòs, Barcelona, Spain.
E-mail address: mtorrell@irec.cat (M. Torrell).
[1] These authors (Elif Kabakci and Natalia Kostretsova) contributed equally to this work

https://doi.org/10.1016/j.jece.2025.116047
Received 15 January 2025; Received in revised form 28 February 2025; Accepted 2 March 2025
Available online 3 March 2025
2213-3437/© 2025 The Authors. Published by Elsevier Ltd. This is an open access article under the CC BY license (http://creativecommons.org/licenses/by/4.0/).

with Ni pellets and spheres [7,8]. The structured reactors are based on a 3D shaped support covered with a layer of active material, which allows pressure drop reduction, heat and mass transfer enhancement, and generally offers superior catalytic performance compared to fixed-bed systems [4]. In this context, honeycomb monoliths represent one of the most common and efficient structured catalyst configurations used for the CO_2 methanation. Conventionally designed monoliths, featuring thin-walled, narrow and parallel channels, enhance the catalytic performance of the system due to low pressure drops, variable catalytic layer thickness, excellent heat and mass transfer, and potential to operate under high gas flow rates [9–11]. Conventionally, monoliths produced by extrusion are constituted by an array of straight and parallel channels, which results in a laminar flow distribution of the reactants during the methanation. Therefore, the kinetics and overall efficiency of the catalytic process are affected by diffusion limitations arising from the geometrical simplicity of the monolith design, which constrains further enhancement of the catalytic performance [12]. Thus, advanced design modifications beyond the capabilities of the conventional manufacturing techniques are essential to improve the flow distribution and boost the performance of the methanation devices [6,8,9].

In recent years, three-dimensional (3D) printing technologies have demonstrated remarkable potential for the design and fabrication of catalytic monoliths with advanced geometries, offering significant enhancements in performance compared to conventional support structures [13,14]. The researchers have highlighted the benefits attained in varying designs for support geometry on the CO_2 methanation conversion performance by studying structured catalysts with non-traditional designs [15–17]. Danaci et al. [18,19] used 3D fiber deposition technology to produce linear and zig-zag structures used as supports for CO_2 methanation. The study demonstrated the successful operation of the 3D printed monoliths with Ni-Al_2O_3 catalyst dip coated on their surface, while 3D structuration of the geometry led to an increase of CO_2 conversion about 40 % at 300°C owing to synergistic improvements in both mass and heat transfer. Baena-Moreno et al. [20] and Gonzalez-Castano et al. [21] have demonstrated the superior catalytic performance of 3D printed metallic supports with gyroid-based geometry with respect to the monoliths with conventional design. In particular, the application of advanced geometry of gyroid structures, characterized with high surface-to-volume ratio, led to an increase of heat and mass transfer rates, along with the generation of turbulent flow within the channels, which significantly enhanced the efficiency of CO_2 methanation processes.

However, most of the studies were focused on the development of the catalytic systems based on 3D printed metallic structured supports, which present several drawbacks with respect to ceramics, including low porosity and high thermal expansion coefficients, which could result in poor adhesion of the catalyst to the monolith surface [22]. Therefore, the development of a reliable 3D printing approach to produce ceramic monoliths is still required. On this frame, recent studies present pioneering applications of ceramic-based 3D printing technologies for manufacturing of structured supports for different catalytic processes, focusing on creating intricate geometries to enhance catalytic activity [23,24]. One example is provided by Liu et al. [25,26] by 3D printing NiMo/Al_2O_3 monoliths with a wall thickness of ~1 mm for hydrodesulfurization process. Further advancements were demonstrated by Zhang et al. [27] by stereolithography (SLA) 3D printing of alumina topologically structured monoliths for dry methane reforming with Ni-based catalysts. This method enabled the production of advanced support structures with intricate features of ~700 μm, resulting in excellent catalytic performance.

Specifically addressing CO_2 methanation processes, Chaparro-Garnica et al. [28] reported the fabrication of carbon monoliths by indirect 3D printing and sol-gel methods. The complex ceramic structure loaded with Ni/CeO_2 catalyst was characterized by enhanced catalytic activity compared to the conventional reactor geometries owing to turbulent flow distribution promoted by 3D structuration of the support design. However, the performance improvement was constraint by the resolution and dimensional accuracy of the selected 3D printed technology. Therefore, further studies are needed for engineering of innovative monolith designs, which offer high surface quality and reproducibility. Another approach was presented by Hajimirzaee et al. [29], who used liquid deposition modelling (LDM) for 3D structuration of cordierite monoliths applied for methane oxidation creation. The enhanced catalytic activity of the system with the 3D printed substrate was attributed to an increase of the turbulence kinetic energy within the reactor owing to the advanced geometry of the 3D printed monolith. Similarly, the design freedom provided by LDM is significantly affected by nozzle diameter, resulting in monolith wall thickness limited to a minimum of 0.59 mm. Zakeri et al. [30] studied the stereolithography 3D printing of alumina-ceria monoliths with straight and twisted hexagonal channels. The study was primarily focused on the feedstock formulation, while no assessment of the catalytic performance was provided. Nevertheless, the research highlighted the capabilities of SLA for the fabrication of innovative self-supported catalytic devices with intricate high-aspect-ratio features and high surface quality. Thus, SLA provides the opportunity for miniaturization of the monolith geometry owing to its high geometrical resolution [31]. Therefore, the application of SLA 3D printing holds an outstanding potential to produce new generation of ceramic structured supports for CO_2 methanation, which was explored and exploited in this work.

This study presents the SLA 3D printing of alumina honeycomb monoliths with advanced design, which were successfully applied for CO_2 methanation using the Ni catalyst. This work investigates the correlation between the geometrical complexity of the 3D printed ceramic support structures and their catalytic efficiency using two distinct monolith types featuring extruded and twisted channel geometry. The influence of support design on reactor performance is further examined with computational fluid dynamics (CFD) analysis, demonstrating the enhancement of the flow distribution achieved by 3D structuration of the monolith geometry. Thus, this work provides a significant contribution to advancing the use of 3D printing technologies in the production of highly efficient catalytic devices, from the modelling to the experimental characterization.

2. Experimental method

2.1. Fabrication of 3D printed monoliths

The monoliths with a total diameter of 12 mm and a height of 10 mm were fabricated by stereolithography. For this purpose, CATIA (Dassault Systèmes, France) software was employed to create computer-aided design (CAD) of two types of complex hierarchical structures formed by hexagonal channels with a diameter of 0.5 mm and 1.15 mm separated by 0.3 mm-thick walls. The traditional honeycomb structure with the straight channels (Type I), which could be fabricated by conventional extrusion technology, was reproduced to enable the comparison with the complex monolith design. An advanced structure with the non-straight channels (Type II) was produced as a vertical array of 1 mm-thick elements twisted by 20°C with respect to each other as shown in the Fig. 1a. Fig. 1b presents both types of monolith designs coded regarding their channel size (0.5- or 1.15-) and shape: extruded (EXT) and twisted (TW).

The monoliths were fabricated by CERAMAKER® C900 SLA 3D printing machine (3DCERAM-Sinto, France) using commercial 3DMIX-AL alumina paste (3DCERAM-Sinto, France) composed of a photosensitive resin and alumina ceramic powder loading. The paste was distributed on the printing platform by two doctor blades (calibrated with 50 mm and 150 mm offset) to create thin and homogeneous layer with a thickness of 50 μm, which was photocured using a UV laser emission (355 nm) according to the CAD design pattern. The laser power was adjusted prior to each printing aiming to achieve a sufficient cure depth value (200 μm), which is essential to ensure the quality of the

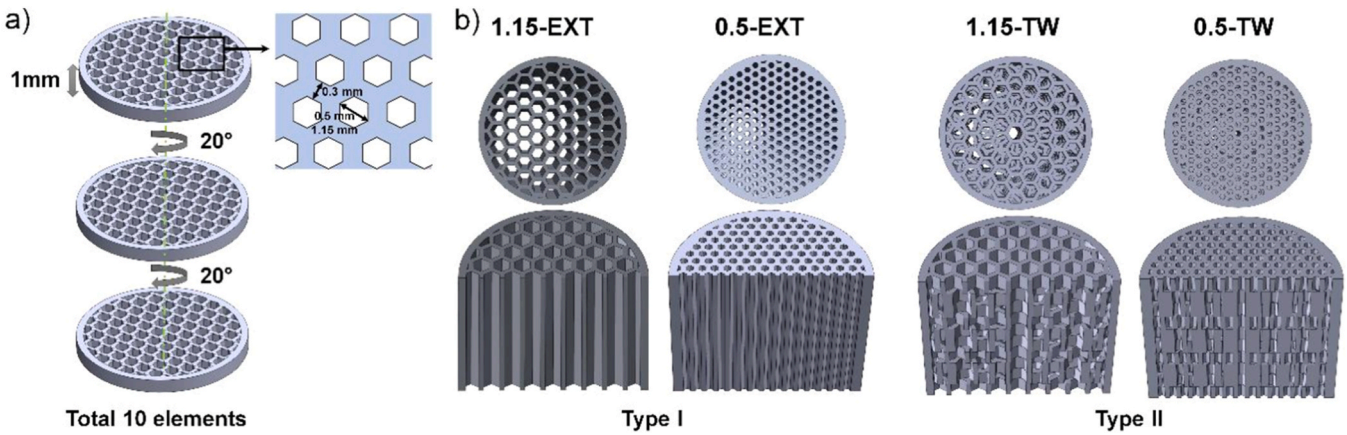

Fig. 1. a) Schematic representation of twisted monolith design concept; and b) Final geometries of Al_2O_3 monoliths with Type I: traditional structure with the straight channels and Type II: advanced structure with the twisted channels at top and cross-sectional views.

process. After the photopolymerization of the current layer, the printing platform was lowered, and a new paste layer was delivered to the printing platform by the doctor blade system. The procedure was repeated until the designed geometric shape is fully formed, as explained in detail in the previous works [32–34]. After the printing, the parts were cleaned from the uncured paste with a wax-based solvent (Ceracleaner®, 3DCERAM-Sinto, France), and thermally treated within a single thermal cycle combining debinding and sintering stages. The organic components, which are present in the feedstock formulation, were thermally removed from the as-printed (green) alumina parts during the debinding process under nitrogen atmosphere performed at temperatures below 800°C, while the dwelling stage for 2 hours was conducted at 800°C to ensure the decomposition of the polymeric matrix. The sintering was performed under synthetic air atmosphere at the temperatures varied from 1200 to 1500°C for 4 h, which was selected as optimal conditions to ensure the sufficient porosity and mechanical stability of the 3D printed support structure.

2.2. Functionalization of the printed monolith alumina supports

In this work, Ni is selected as the active metal, because it is commonly applied as a catalyst owing to its high activity and relatively low price [35]. The deposition of the nickel active phase on the surface of the sintered alumina monoliths was performed by wet impregnation method. The alumina supports were immersed in a 4 M $Ni(NO_3)_2{\cdot}6H_2O$ aqueous solution for 2 h and dried in an atmospheric oven at 100°C overnight. Subsequently, the catalyst underwent calcination at 450°C for 1 h with a heating ramp of 3°/min in air. The quantification of NiO attached to each 3D printed monolith was determined by weighing the supports before impregnation and after the calcination stages [36,37]. Solid surface area attributed to each monolith design was estimated using CATIA CAD software [38].

2.3. Material characterization

XRD analysis of a monolith was performed on a Bruker D8 diffractometer (Bruker Corporation, USA) (Cu K_α, $\lambda = 1.5406$ Å) at 40 kV and 40 mA, scanning 20° to 80° in θ/2θ geometry with a 0.020° step size. The microstructural characterization was made using a Scanning Electron Microscope Auriga (Zeiss, Germany) with Schottky emitter, 30 kV FESEM column equipped with an energy dispersive X-ray (EDX) detector (Oxford Instruments, UK). The samples were sputter-coated with a thin layer of gold before imaging. Nitrogen adsorption/desorption analysis (BET) was carried out on a Tristar II 3020 analyzer (Micrometrics Instrument Corporation, USA) at 77 K. The Brunauer-Emmett-Teller (BET) method was applied to calculate the BET surface area (see supplementary information section S1), and the average pore size was determined using the Barrett-Joyner-Halenda (BJH) method. The porosity of 3D printed and sintered supports was estimated considering their bulk density and theoretical density of alumina.

2.4. Catalytic performance evaluation

Catalyst activity, selectivity and stability tests were carried out in a laboratory scale fixed-bed catalytic reactor with an internal diameter of 13 mm and 305 mm length. The reaction temperature was controlled with a K-type thermocouple placed above the sample inside of the reactor. The reactant gases H_2 (99.999 %, Linde Gas España, Spain) and CO_2 (99.999 %, Linde Gas España, Spain) were regulated using mass flowmeter controllers (MFC, Bronkhorst, Netherlands).

Prior to starting the methanation test, the catalysts deposited on the monolith samples was reduced in-situ under H_2 flow (100 N mL/min) at 500°C with a ramp of 1 °C/min for 3 h and, subsequently, cooled down to 50°C. After that, methanation tests were carried out under a gas flow of H_2:CO_2 with stoichiometric molar ratio of 4:1. The operating conditions included a pressure of 5 bar·g and gas flow rates (F) ranging from 25 to 200 N mL/min. The catalyst screening was performed within a temperature range of 300–475°C, at intervals of 25°C, starting from the lowest temperature. Following the reaction, the output gases were separated from water with the help of a cold liquid gas separator (5°C), enabling dry flow measurement with a mass flow meter (MF, Bronkhorst, Netherlands). Then, the composition of this dry gas was determined using a 490 micro chromatograph (Agilent Technologies, USA) analyzing the presence of CH_4, H_2, CO, CO_2 and C_2H_6 in the product mixture. An average value of three measurements was taken at each temperature, with a relative error of ± 2 %. Stability tests were carried out at a constant temperature of 400°C, a pressure of 5 bar·g, and F = 300 N mL/min, with the output composition monitored every hour for 24 hours.

The CO_2 conversion and CH_4 selectivity were calculated using the Eqs. (2) and (3):

$$X_{CO_2} = 1 - \frac{F_{CO_2,\,out}}{F_{CO_2,\,in}}.100 \tag{2}$$

$$S_{CH_4} = \frac{F_{CH_4,\,out}}{F_{CH_4,\,out} + F_{CO,\,out}}.100 \tag{3}$$

where $F_{CO_2,\,in}$ and $F_{CO_2,\,out}$ are the molar flow rates of CO_2 at the reactor inlet and outlet, respectively, $F_{CH_4,\,out}$ is the outlet molar flow rate of CH_4, detected by MFC and MF, respectively.

2.5. CFD simulation

To investigate the effect of design on fluid dynamics, turbulence and velocity profile were analyzed, using ANSYS Fluent software, 2022.R2 version. A CFD study was performed using a three-dimensional domain that replicates the design of a single channel of each monolith type (Fig. 2). The symmetric nature of both geometry and boundary conditions allowed to approximate an entire monolith structure as an individual channel. In this case, the model accurately captures the flow characteristics of the system, while enabling high-resolution simulations to be performed within a reasonable computational time. The hexagonal channels with the size of 0.5 mm were selected for the simulation of the flow behavior for both types of the monolith designs. The geometry employed for the simulation of the reference Type I monolith represented a 10 mm-long straight hexagonal channel. The monoliths of the Type II were simulated with a single 10 mm-long channel formed by an array of ten 1 mm-thick hexagonal elements twisted by 20° with respect to each other. Thus, the selection of the model geometries allows the deep exploration of differences in flow characteristics specifically attributable to the channel design.

The single twisted and extruded shape tubes were plotted in the XY plane, and the fluid flowed along the Z axis. The CFD analysis was performed using the realizable k-epsilon model with default constants. This model is particularly suitable for predictions of different flow conditions, such as spreading rates, rotational flows, and complex structures [39]. The behavior of the flow was simulated using transport equations for turbulent kinetic energy (k) and turbulence dissipation rate (ϵ) as outlined in the study by Hajimirzaee et al. [29]. Gas mixture of a H_2:CO_2 with stoichiometric molar ratio of 4:1 was used as the fluid, as required for Sabatier. The simulation was carried out with an inlet gas velocity of 0.0295 m/s (corresponding to Gas Hourly Space Velocity (GHSV) of 10620 h^{-1}), an outlet gauge pressure of 0 Pa, and at the temperature of 400°C, selected as boundary conditions [40]. The resolution of the mesh was selected according to the channel design to maintain the high accuracy of the simulated results, which included more than 74000 and 280000 finite elements for the extruded (Type I) and twisted (Type II) geometries, respectively.

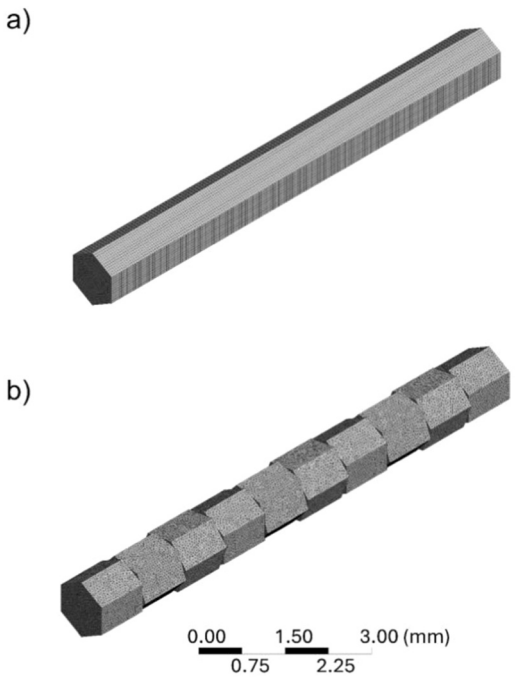

Fig. 2. Fluid domain mesh for CFD analysis of the catalytic system based on different monolith designs: a) Type I – extruded channel with the size of 0.5 mm (0.5-EXT), b) Type II – twisted channel with the size of 0.5 mm (0.5-TW).

3. Results and discussion

3.1. Characterization of 3D printed monoliths

The performance of catalytic systems, which consist of an active metallic phase and a support structure, is affected by different factors, such as the selection of the materials and geometry of the reactor. From this perspective, the monolith is considered as a substrate for the catalyst layer, which defines the gas and heat distribution inside the system. In this regard, the microstructure of ceramic monoliths is a key factor to ensure the attachment of the catalyst to the substrate surface, which is essential for high catalytic activity of the reactor. Uniform dispersion of the catalytically active component on the monolith should be achieved by controlling the surface quality, the deposition process, and the surface chemistry of the support. At the same time, the support structure should exhibit sufficient mechanical stability to be placed in the reactor and operate under a fixed pressure [10,41].

The influence of the sintering temperature on the microstructure and surface quality of the 3D printed alumina-based structured supports was studied by sintering at different temperatures. For this goal, the porosity and BET surface area of 3D printed parts sintered at 1200°C, 1300°C and 1500°C were evaluated, while specific attention was paid to the pore distribution characterization in terms of the amount, size, and volume. The minimum density of 2.5 g/cm^3 was achieved on the sample sintered at 1200°C, while a gradual increase of the value to 2.6 and 3.0 g/cm^3 was obtained by increasing the temperature to 1300°C and 1500°C, respectively. It was shown that 3D printed ceramics sintered at lower temperatures exhibited higher porosity values (37.7 % at 1200 °C and 34.5 % at 1300°C) compared to the monoliths sintered at 1500°C (24.6 %). A similar trend was observed for the N_2-physisorption results, where BET surface area decreased from 2.35 m^2/g at 1200 °C, to 1.80 at 1300 °C and 0.92 m^2/g at 1500 °C, respectively. Moreover, the pore volume was reduced by ~33 % and ~67 % owing to the corresponding increase of the sintering temperature. The structural properties of the 3D printed alumina ceramics are summarized in Table 1. Overall, a balance between reasonable porosity and mechanical robustness necessary for the device operation was found at 1300 °C.

After the sintering, defect-free structured catalysts of both design types were produced, while all geometrical elements could be clearly distinguished, which demonstrates the reliability of the developed approach based on SLA 3D printing. Moreover, the hexagonal cells appear to be well-connected to each other, with no crack formation detected on the internal walls of the monoliths (Fig. 3a).

The molarity of the impregnation solution was optimized to achieve the amount of catalyst, which could be sufficient for the efficient reactor operation (~10 wt% regarding the literature [42,43]), which was homogeneously distributed on the monolith surface without the channel blockage. A 4 M concentration was chosen to meet all the mentioned requirements. After the impregnation process, the surface of the supports is uniformly covered with catalyst material as shown in Fig. 3b.

The presence of NiO phase on the surface of all 3D printed monoliths after the infiltration and calcination procedure is confirmed by XRD analysis (see supplementary information section S2). Table 2 shows geometrical surface area of the 3D printed monoliths and the NiO amount, which is present at the substrate surface after the impregnation,

Table 1
Microstructural properties of sintered alumina monolith samples.

Sintering Temperature (°C)	Sintered bulk density (g/cm^3)	Calculated porosity (%)	BET surface area (m^2/g)	Pore volume (cm^3/g)	Pore size (nm)
1200	2.47	37.7	2.35	0.006	11.7
1300	2.61	34.5	1.80	0.004	11.6
1500	3.01	24.6	0.92	0.002	10.0

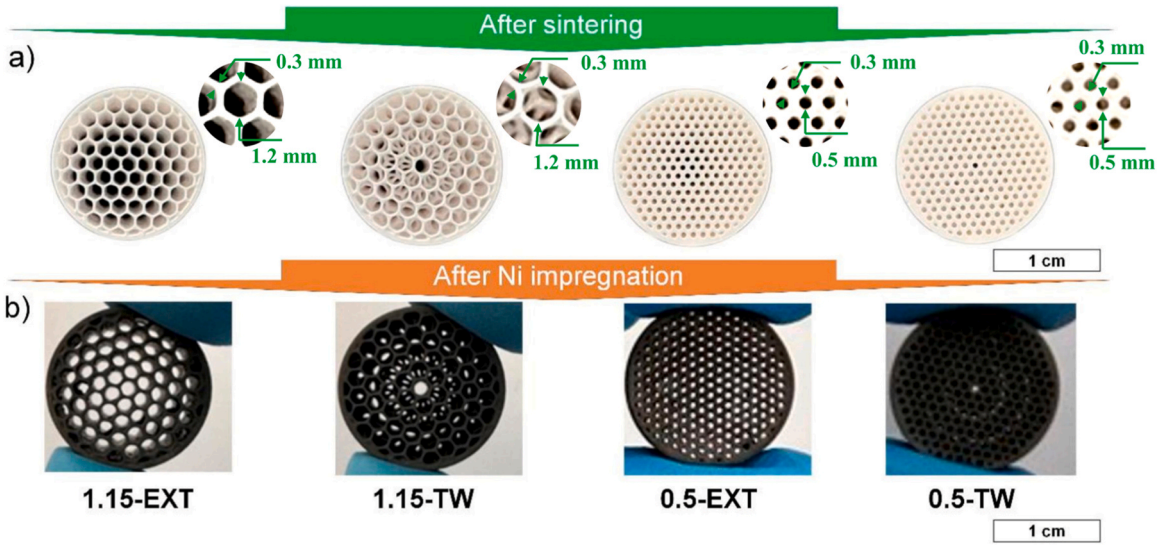

Fig. 3. Top view of 3D printed extruded and twisted honeycomb monoliths: a) Sintered and b) After the catalyst deposition.

Table 2
Structural and physical properties of the 3D printed monoliths.

Sample name	Surface Area (mm^2)	NiO (wt%)
1.15-EXT	3015	7.9
1.15-TW	3428	8.5
0.5-EXT	3655	5.1
0.5-TW	4048	5.9

as it was estimated by weighting the catalytic support before and after the catalyst deposition. The 1.15-EXT (Type I) and 1.15-TW (Type II) designs are characterized with the surface area of 3015 mm^2 and 3428 mm^2, respectively, alongside NiO percentages of 7.9 wt% and 8.5 wt%, which is close to the target value of 10 wt%. The reduction of the channel size to 0.5 mm led to an increase of the surface area for both extruded and twisted monolith geometries (3655 mm^2 and 4048 mm^2, respectively). Therefore, the design strategy that combines both the twisting of the monolith geometry and the reduction of the channel size represents an efficient way to increase the surface area for ~34 %, considering the simplest (1.15-EXT) and intricate (0.5-TW) designs. These results suggest that increasing the geometric complexity of the monolith can enhance the surface area available for catalytic reactions, addressing the limitations of low porosity, which are associated with poor dispersion of active sites. A moderate decrease of the catalyst loading detected for 0.5-EXT and 0.5-TW monoliths (5.1 % and 5.9 %, respectively) was considered as a result of the channel size reduction from 1.15 to 0.5 mm, affecting the interaction between the active phase and support material.

The microstructures of the 0.5-EXT and 0.5-TW monoliths after the methanation and stabilization test are presented in Figs. 4a and 4b, respectively. Both types of the 3D printed supports exhibited distinct 0.5-mm hexagonal elements with no defect formation after the operation. The surface of the alumina substrates was uniformly covered with Ni particles with an average size of ~300 nm, while no agglomeration of Ni particles was detected. The EDX element mapping (Fig. 4c) proved a homogeneous distribution of active metal particles on the 3D printed substrates. The uniform distribution of Ni particles across the surface of the 3D printed monoliths indicates good metal-support interaction, which is crucial for catalyst stability and longevity.

To examine the crystalline phases of the catalyst active phase, XRD analysis was performed for the monoliths before and after Ni reduction, as shown in Fig. 5 for the 0.5-EXT monolith. The deposited catalyst material presents the characteristic peaks of NiO at 37°, 43°, and 63° corresponding to the (111), (200), (220) diffraction planes (Fig. 5a). The active material is fully reduced to Ni after the reduction process carried out prior to the methanation test, which is confirmed by the detection of the characteristic peaks of metallic Ni at 44.5°, 51.8° and 76.3° attributed to the (111), (002), (220) diffraction planes (Fig. 5b). Note that the major presence of α-alumina in the phase composition of the 3D printed support, which is less favorable for catalytic applications compared to γ-alumina, could indicate the necessity of CeO_2 addition to the composition of the catalyst active layer (Ni-CeO_2) for further enhancement of the catalytic performance of the system [42].

3.2. Study of the catalytic performance of the printed monoliths

The catalytic performance of extruded and twisted 3D-printed monolithic devices, with varying honeycomb element sizes, was evaluated by measuring CO_2 conversion in the methanation reaction. Fig. 6a presents the results depending on the temperature in the range of 300 – 475 °C under a fixed flow rate of 200 N mL/min. The curve presents a typical behavior attributed to the exothermic CO_2 methanation process [44]. An increase in CO_2 conversion is observed with the increase of the temperature up to 400 °C, where the control of the reaction is controlled by kinetic factors. At the temperatures beyond 425 °C the equilibrium conditions of the reactions are reached, where the process is thermodynamically limited [45].

All studied monolith designs present high CO_2 conversion values, above 70 %, at 400 °C. The reduction of the hexagonal element size from 1.15 to 0.5 mm results in the enhancement of the catalytic performance for both design types (from 73 % to 80 % for extruded monoliths, and from 80 % to 84 % for the twisted ones).

Note that the reduction of the Ni content, detected after the deposition and calcination of the catalyst layer, does not hinder the performance of the supports. In this regard, the reduction of the hexagonal element size offers the possibility to reduce the utilization of the valuable catalyst material, while maintaining high catalytic performance. This could be beneficial for the manufacturing of large-scale devices, which require an optimization of the production cost and responsible resource utilization, while decreasing the environmental impact of the toxic material usage.

Twisting of the geometry leads to an improvement of the catalytic activity. In particular, an increase of ~9 % is reported for the CO_2 conversion using the 1.15-TW monolith with respect to the 1.15-EXT support. The same trend is observed for the substrate designs with smaller hexagonal elements, which results in an increase from 80 % to

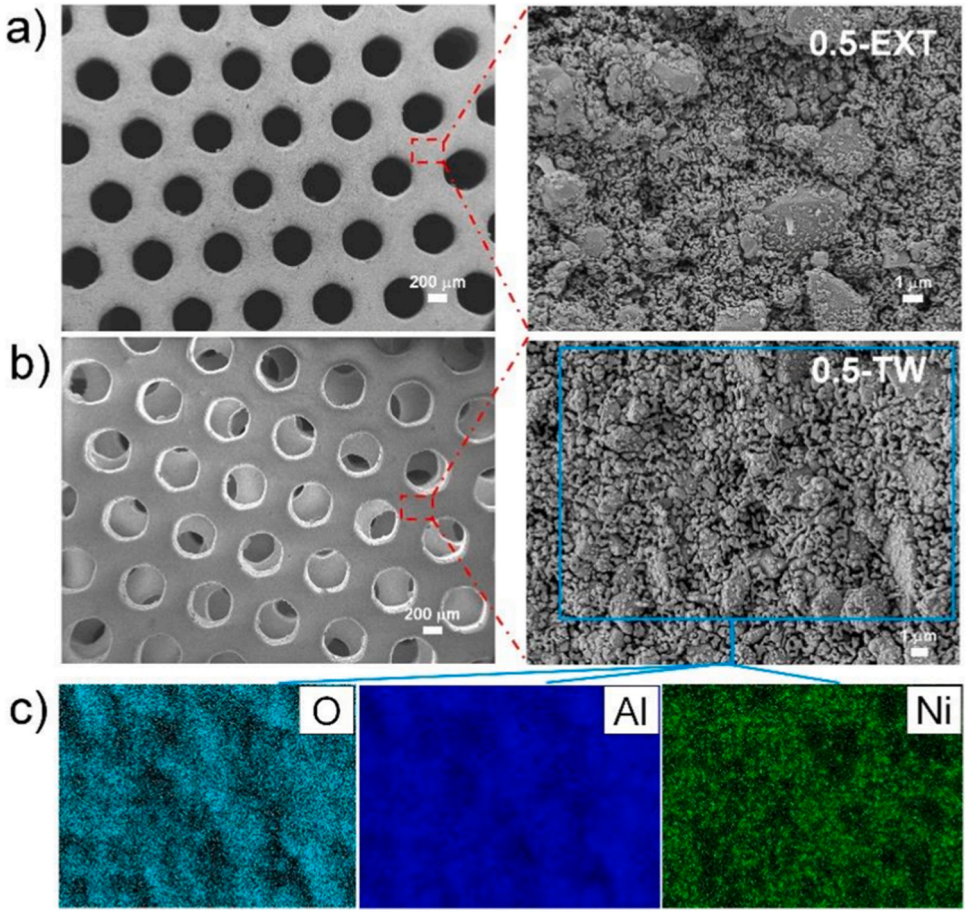

Fig. 4. SE-SEM images of a) 0.5-EXT, b) 0.5-TW monoliths at different magnifications after the catalyst reduction, and evaluation of the catalytic performance of the system, c) EDX elemental mapping images of the 0.5-TW monolith.

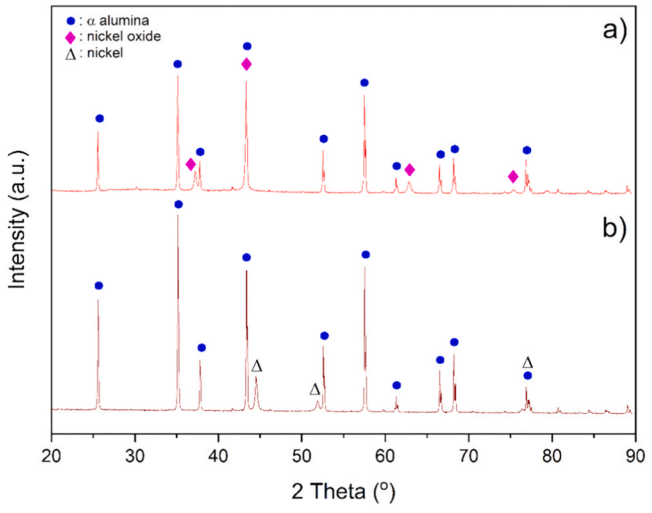

Fig. 5. XRD patterns of 0.5-EXT monolith after a) Ni impregnation and calcination; b) Reduction at 500°C. JCPDS-card number: NiO (00–022–1189), Ni (00–001–1260), α-Al_2O_3 (01–082–1467).

84 % (0.5-EXT and 0.5-TW, respectively). The obtained CO_2 conversion efficiency exceeds the values reported for the state-of-the-art reactors based on the conventionally fabricated monoliths [19,46–48]. In particular, Vita et al. [46] developed a catalytic system using cordierite monoliths coated with a Ni catalyst supported by gadolinia-doped ceria, achieving ~70 % CO_2 conversion at 400 – 450 °C (GHSV: 10000 h^{-1}). Similarly, Navarro et al. [49] demonstrated a reactor based on FeCrAlloy monolith coated with a Ru-Ni/$MgAl_2O_4$ catalyst, which achieved a ~60 % CO_2 conversion at 400 °C (gas flow rate: 200 NmL/min). In this context, the 3D printed alumina monoliths with the twisted geometry and 0.5 mm channels exhibits a 20 % and 40 % improvement in CO_2 methanation performance with respect to conventional ceramic and metallic monoliths, respectively, under similar operation conditions. Thus, the 0.5-TW structured support, which exhibits the highest CO_2 conversion values of 84 % at 400 °C and 89 % at 425 °C, highlights the strong relationship between the design complexity and catalytic efficiency for the 3D printed alumina monoliths. The improvement in the catalytic performance achieved for the structured supports with the twisted channel geometry could be associated with an improvement of the flow distribution, achieved due to the non-linear shape of the hexagonal channels. Fig. 7a presents a simulated profiles of the gas velocity magnitude distribution along the straight and twisted monolith channel, while the pressure distribution along the channel is shown in the supplementary information section (S3). It is shown that the here-proposed modification of the channel geometry leads to an increase of the velocity gradient of the reactants compared to the conventional extruded shape, which improves the diffusion of the reactants from the bulk to the active sites [50], and, thus, could facilitate the mass transport across the system. In this sense, the formation of heterogeneous gas flow leads to a decrease of the near-wall boundary layer thickness, as it is detected for the monoliths with the twisted channels, which enhances the reactant diffusion to the catalyst surface [51]. Moreover, twisting of the channel geometry promotes the formation of turbulences distributed along the non-straight reactant gas path, as shown in the Fig. 7b. In this regard, the

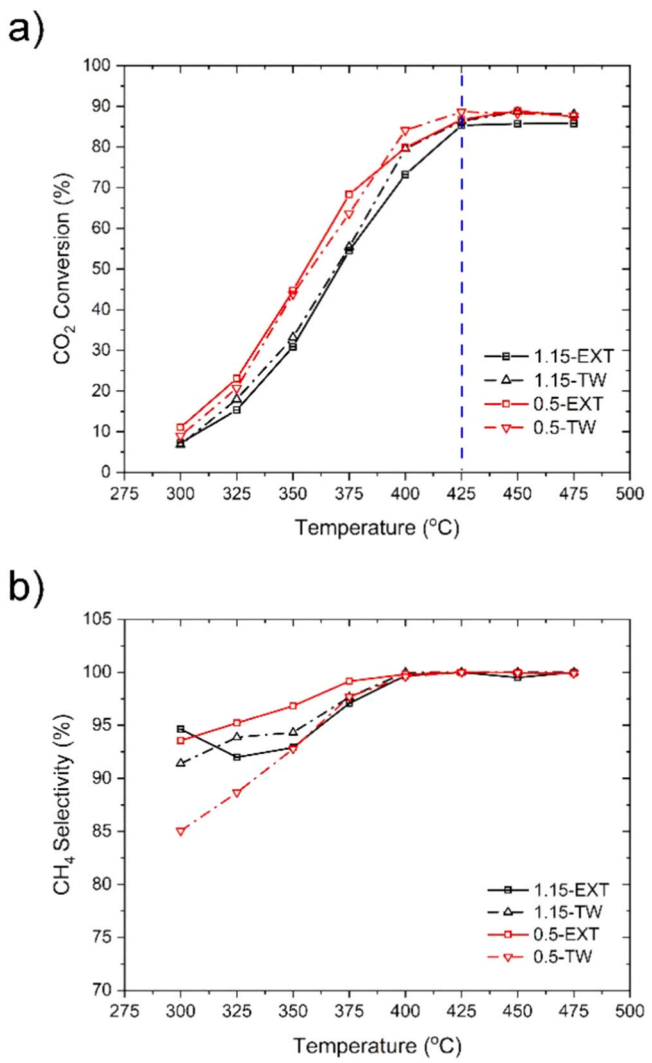

Fig. 6. a) CO_2 conversion vs. temperature and b) CH_4 selectivity vs. temperature for the catalytic systems based on the 3D printed alumina monoliths. F = 200 N mL/min.

turbulence in the reactant flow promoted by the monolith geometry, not only improves the mass transport of the reactants, but also favors the heat release from the system, preventing the formation of hot spots [16, 52,53]. In total, the twisting of the honeycomb channels significantly enhances the interaction of the reactants with the active catalyst phase deposited on the monolith walls, which results in an increase of the catalytic efficiency of the system compared to the conventional geometries.

The CH_4 yield above 80 % is obtained in the investigated temperature range, which is considered a relatively high value with respect to conventional Ni-Al_2O_3 catalytic systems [6]. The CH_4 selectivity increases with temperature and a maximum of 100 % is reached at 425 °C for all designs, showing high catalytic efficiency of the system based on the 3D printed alumina monoliths (Fig. 6b).

Fig. 8 presents the CO_2 conversion values at 400°C at different flow rates ranging from 25 to 200 NmL/min. A clear dependence between the reactant flow, monolith design, and catalytic efficiency is proved. An increase of the CO_2 conversion corresponds to a decrease of the flow rate, reaching a maximum at 25 N mL/min, which could be associated with a lower residence time at higher velocities [49].

Moreover, the support geometry has a clear impact on the catalytic performance. Both structured supports with smaller size of the hexagonal elements exhibit higher CO_2 conversion in the entire range of the flow rates, since the optimal velocity distribution could be achieved by the reduction of the monolith channel width below 1 mm [54]. The study shows that the combination of channel size reduction with the twisting of the monolith geometry leads to a significant increase in the catalytic activity. The 0.5-TW monolith design consistently presents higher CO_2 conversion values compared to other investigated geometries, which is associated with an increase of contact time due to the 3D structuration of the geometry. The difference is especially pronounced at higher velocities by reaching ~84 % CO_2 conversion at 200 N mL/min. Therefore, the application of advanced structured catalytic support produced by 3D printing particularly well-suited for large-scale industrial systems, which operate at higher flow velocity values [30]. Overall, the CO_2 conversion of the 3D printed 0.5-TW monolith exceeds 90 % at the flow rates below 100 NmL/min, representing a significant enhancement compared to the conventional systems based on ceramic monoliths operating under similar conditions. Particularly, Ricca et al. [55] presented a reactor based on a SiC monolith functionalized with Ni/Al_2O_3 or Ni/CeO_2 catalysts, which exhibited a CO_2 conversion of ~70 % (Ni/Al_2O_3) and ~80 % (Ni/CeO_2) at 400 °C under a flow rate of 30 $L{\cdot}g_{cat}{\cdot}h^{-1}$, which corresponds to 50 NmL/min used in the present study. Parra-Marfil et al. [56] developed a system based on a cordierite monolith coated with a Ni/CeO_2 catalyst, reaching ~80 % efficiency at 400 °C under a flow rate of 100 NmL/min. Thus, the 3D structuration of the monolith geometry via additive manufacturing improves reactor catalytic efficiency by more than 15 % compared to state-of-the-art devices operating at low gas flow rates.

Stability tests were carried out for the catalytic systems with the 0.5-TW and 0.5-EXT 3D printed monoliths. For this purpose, the CO_2 conversion values are monitored at 400 °C and a flow rate of 300 N mL/min for 24 hours (Fig. 9). The catalytic activity does not present any significant differences during the investigated period of the continuous operation, while the conversion values remain around 62 %, reflecting high stability of the system based on the 3D printed alumina structured supports. In total, the application of 3D printed alumina monoliths demonstrated an outstanding potential to enhance the performance of the CO_2 methanation reaction. The increase of geometrical complexity by twisting the honeycomb structure and reduction of the hexagonal element size represents a promising way to improve CO_2 conversion, particularly at high flow rates.

4. Conclusions

Stereolithography 3D printing was successfully used to fabricate alumina structured supports for CO_2 methanation. Two types of monolith designs based on the extrusion and twisting of the honeycomb geometry with 1.15-mm and 0.5-mm hexagonal elements were produced by SLA and sintered at 1300 °C. The twisted-shaped monoliths exhibited an increase of the surface area, resulting in higher Ni load compared to the extruded designs. The implementation of narrower channels (0.5 mm) led to a decrease of the Ni load for both designs. Therefore, the proposed monolith designs allow the reduction of the Ni load while maintaining a high methane yield, benefiting both material usage and reactor production costs. The highest CO_2 conversion of 84 % and 89 % at 400 and 425 °C, respectively, was obtained for the twisted monolith design with 0.5 mm hexagonal cells. The geometrical complexity of the support had a critical impact on the catalytic activity of the system when operating at high gas flow rates, as higher CO_2 conversion is achieved owing to the advanced monolith geometry. The corresponding improvement was attributed to the enhancement of the flow distribution by turbulence formation and facilitation of mass transport achieved by the 3D structuration of the reaction channels, as confirmed by CFD analysis. The continuous operation of the catalytic system is reported for 24 h at 400 °C, proving the overall stability of the 3D printed monoliths to CO_2 methanation process. These results demonstrate a direct performance enhancement as a result of the application of additive manufacturing technology for catalytic support fabrication.

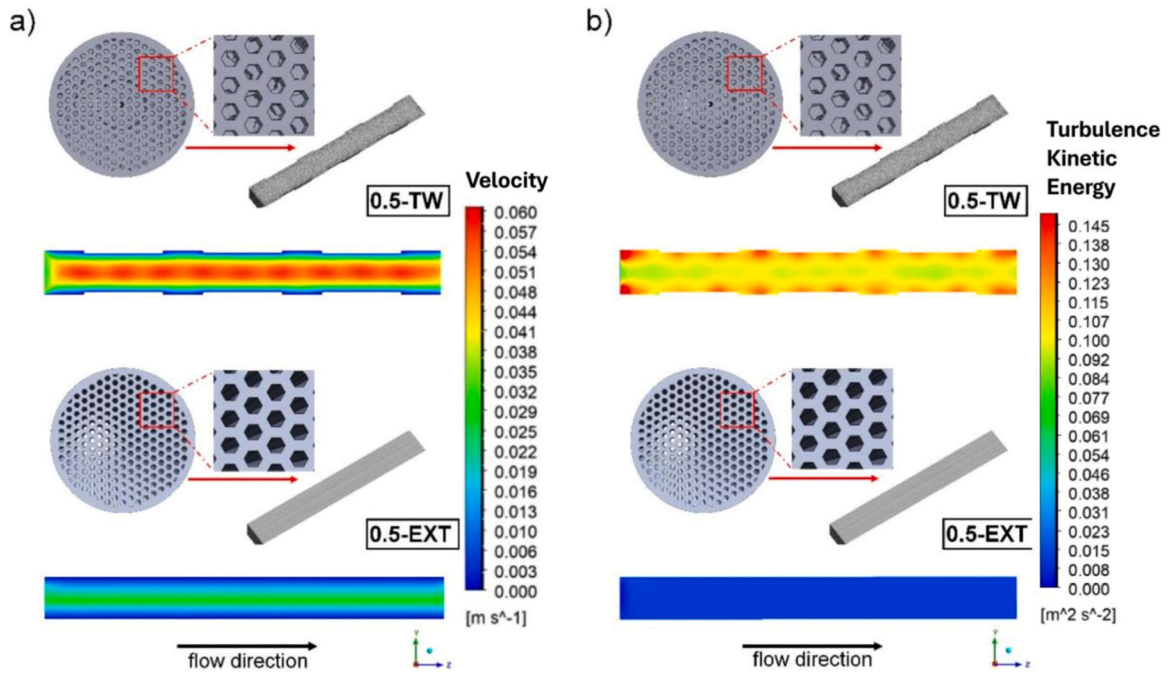

Fig. 7. a) Velocity contour and b) Turbulence kinetic energy contour along extruded channel with the size of 0.5 mm (0.5-EXT) and twisted channel with the size of 0.5 mm (0.5-TW).

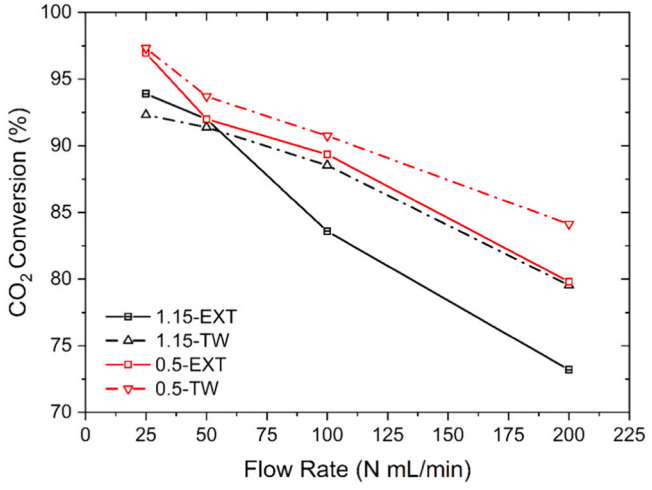

Fig. 8. CO_2 conversion vs. flow rate for four monoliths tested.

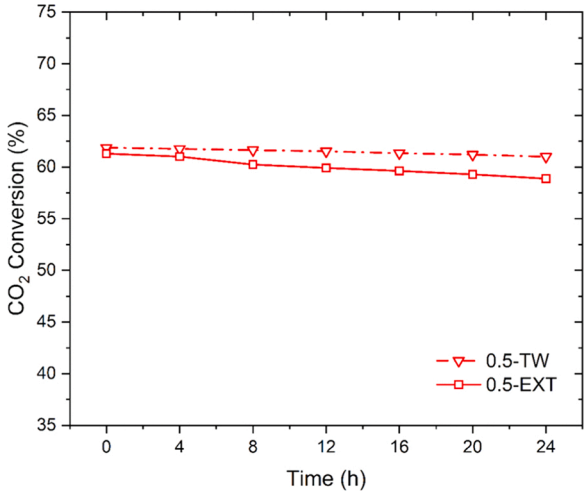

Fig. 9. CO_2 conversion (%) in 24 h stability tests of 0.5-TW and 0.5-EXT samples at 300 N mL/min flow rate. H_2:CO_2= 4:1 (mol), P = 5 bar.

Thus, the developed innovative approach represents a significant advancement in the field of catalyst design and fabrication for CO_2 methanation. This method allows for the direct production of intricate catalyst structures in a single step, overcoming limitations of previously developed multi-step processes or substrate-focused approaches. Therefore, this study opens a new pathway for the fabrication of the structured catalytic supports by means of 3D printing tailoring the design of the monoliths for the potential application in large-scale or high-throughput systems.

CRediT authorship contribution statement

Kabakci Elif: Writing – original draft, Visualization, Investigation, Formal analysis, Conceptualization. **Kostretsova Natalia:** Writing – review & editing, Investigation, Formal analysis. **Martín Morales Elena:** Writing – review & editing, Methodology, Investigation, Formal analysis, Conceptualization. **Diaz-Ruiz Jesús:** Investigation. **Tarancón Albert:** Writing – review & editing, Supervision, Funding acquisition, Conceptualization. **Guilera Jordi:** Writing – review & editing, Supervision, Methodology, Formal analysis, Conceptualization. **Torrell Marc:** Writing – review & editing, Supervision, Funding acquisition, Formal analysis, Conceptualization.

Declaration of Competing Interest

The authors declare that they have no known competing financial interests or personal relationships that could have appeared to influence the work reported in this paper.

Acknowledgements

This project has received fundings from the Government of Catalonia, the Secretariat for Universities and Research of the Ministry of

Business and Knowledge of the Government of Catalonia and the European Social Fund. (2021 SGR 00750 and 2021 FI_B 00984). The research leading to these results has received financial support in the frame of FASSION3D (PID2022–137626OB-C32) and VALOTAIL (PID2023–151777OB-I00) projects funded by MCIN/AEI/10.13039/501100011033/ FEDER, UE. Additionally, this work was supported by the Scientific and Technological Research Council of Türkiye (TUBITAK) through the 2219-International Postdoctoral Research Fellowship Program (Grant number: 1059B192201288).

Appendix A. Supporting information

Supplementary data associated with this article can be found in the online version at doi:10.1016/j.jece.2025.116047.

Data Availability

Data will be made available on request.

References

[1] P. Błaszczak, M. Zając, A. Ducka, K. Matlak, B. Wolanin, S.F. Wang, A. Mandziak, B. Bochentyn, P. Jasiński, High-temperature co-electrolysis of CO_2/H_2O and direct methanation over co-impregnated SOEC. Bimetallic synergy between Co and Ni, Int. J. Hydrog. Energy 47 (82) (2022) 35017–35037.
[2] M. Götz, J. Lefebvre, F. Mörs, A. McDaniel Koch, F. Graf, S. Bajohr, R. Reimert, T. Kolb, Renewable power-to-gas: a technological and economic review, Renew. Energy 85 (2016) 1371–1390.
[3] Tanja Schaaf, et al., Methanation of CO_2-storage of renewable energy in a gas distribution system, Energy, Sustain. Soc. 4 (1) (2014) 1–14.
[4] J.C. Navarro, M.A. Centeno, O.H. Laguna, J.A. Odriozola, Policies and motivations for the CO_2 valorization through the sabatier reaction using structured catalysts. A review of the most recent advances, Catalysts 8 (12) (2018) 1–25.
[5] C. Vogt, M. Monai, G.J. Kramer, B.M. Weckhuysen, The renaissance of the sabatier reaction and its applications on earth and in space, Nat. Catal. 2 (3) (2019) 188–197.
[6] C. Lv, L. Xu, M. Chen, Y. Cui, X. Wen, Y. Li, Q. Shou, Recent progresses in constructing the highly efficient Ni based catalysts with advanced low-temperature activity toward CO_2 methanation, Front. Chem. 8 (2020) 269.
[7] G. Groppi, E. Tronconi, Honeycomb supports high thermal conductivity for gas/solid chemical processes, Catal. Today 105 (3-4) (2005) 297–304.
[8] E. Tronconi, G. Groppi, C.G. Visconti, Structured catalysts for non-adiabatic applications, Curr. Opin. Chem. Eng. 5 (2014) 55–67.
[9] A. Cybulski, J.A. Moulijn, Monoliths in heterogeneous catalysis, Catal. Rev. Sci. Eng. 36 (2) (1994) 179–270.
[10] S. Hosseini, H. Moghaddas, S.M. Soltani, S. Kheawhom, Technological applications of honeycomb monoliths in environmental processes: a review, Process Saf. Environ. Prot. 133 (2020) 286–300.
[11] F. Kapteijn, J.A. Moulijn, Structured catalysts and reactors–perspectives for demanding applications, Catal. Today 383 (2022) 5–14.
[12] I. Fuentes, J.P. Mmbaga, A. Blanco, R.E. Hayes, F. Gracia, Kinetic model of CO_2 methanation in a microreactor under power-to-gas conditions, J. CO_2 Util. 75 (2023) 102552.
[13] H.L. Huynh, Z. Yu, CO_2 methanation on hydrotalcite-derived catalysts and structured reactors: a review, Energy Technol. 8 (5) (2020) 1901475.
[14] O.H. Laguna, P.F. Lietor, F.J.I. Godino, F.A. Corpas-Iglesias, A review on additive manufacturing and materials for catalytic applications: milestones, key concepts, advances and perspectives, Mater. Des. 208 (2021) 109927.
[15] J.J. Bolívar Caballero, T. Han, R. Svanberg, I.N. Zaini, H. Yang, R. Gond, P. Cao, T. Lewin, P.G. Jönsson, W. Yang, Advanced application of a geometry-enhanced 3D-printed catalytic reformer for syngas production, Energy Convers. Manag. 287 (March) (2023) 117071.
[16] Y. Li, S. Chen, X. Cai, J. Hong, X. Wu, Y. Xu, B.H. Chen, Rational design and preparation of hierarchical monoliths through 3D printing for syngas methanation, J. Mater. Chem. A 6 (14) (2018) 5695–5702.
[17] J.J.B. Caballero, T. Han, R. Svanberg, I.N. Zaini, H. Yang, R. Gond, W. Yang, Advanced application of a geometry-enhanced 3D-printed catalytic reformer for syngas production, Energy Convers. Manag. 287 (2023) 117071.
[18] S. Danaci, L. Protasova, J. Lefevere, L. Bedel, R. Guilet, P. Marty, Efficient CO2 methanation over Ni/Al_2O_3 coated structured catalysts, Catal. Today 273 (2016) 234–243.
[19] S. Danaci, L. Protasova, F. Snijkers, W. Bouwen, A. Bengaouer, P. Marty, Innovative 3D-manufacture of structured copper supports post-coated with catalytic material for CO_2 methanation, Chem. Eng. Process. Process. Intensif. 127 (2018) 168–177.
[20] F.M. Baena-Moreno, M. Gonzalez-Castano, J.C. Navarro de Miguel, K.U. Miah, R. Ossenbrink, J.A. Odriozola, H. Arellano-Garcia, Stepping toward efficient microreactors for CO_2 methanation: 3D-printed gyroid geometry, ACS Sustain. Chem. Eng. 9 (24) (2021) 8198–8206.
[21] M. González-Castaño, F. Baena-Moreno, J.C.N. De Miguel, K.U. Miah, F. Arroyo-Torralvo, R. Ossenbrink, H. Arellano-García, 3D-printed structured catalysts for CO2 methanation reaction: advancing of gyroid-based geometries, Energy Convers. Manag. 258 (2022) 115464.
[22] L. Baharudin, M.J. Watson, Monolithic substrate support catalyst design considerations for steam methane reforming operation, Rev. Chem. Eng. 34 (4) (2018) 481–501.
[23] Z. Chen, Z. Li, J. Li, C. Liu, C. Lao, Y. Fu, Y. He, 3D printing of ceramics: a review, J. Eur. Ceram. Soc. 39 (4) (2019) 661–687.
[24] U. Scheithauer, E. Schwarzer, G. Ganzer, A. Kornig, W. Becker, E. Reichelt, A. Michaelis, Micro-reactors made by lithography-based ceramic manufacturing (LCM), Addit. Manuf. Strateg. Technol. Adv. Ceram. Ceram. Trans. 258 (258) (2016) 31–41.
[25] J. Zhu, J. Liu, J. Zhu, S. Lu, R. Yan, K. Cheng, H. Cheng, H. Liu, H. Li, W. Zhu, 3D printing technique fortifies the ultradeep hydrodesulfurization process of diesel: a journey of NiMo/Al2O3-MMT, Inorg. Chem. 62 (49) (2023) 20050–20061.
[26] J. Liu, J. Zhu, J. Zhu, J. Xu, H. Liu, M. Hua, H. Cheng, H. Li, J. Liu, W. Zhu, H. Ji, One-pot three-dimensional printing of a hierarchical NiMo/Al2O3 monolithic catalyst for 4,6-dimethyldibenzothiophene hydrodesulfurization, ACS Appl. Mater. Interfaces 15 (28) (2023) 33593–33604.
[27] J. Zhang, G. Zhang, J. Song, F. Yu, N.H. Wong, J. Sunarso, N. Yang, B. Meng, X. Tan, S. Liu, Highly stable 3D-printed monolithic Al2O3-supported Ni-based structured catalysts for dry reforming of methane, Addit. Manuf. 80 (October 2023) (2024) 103983.
[28] C.Y. Chaparro-Garnica, E. Bailón-García, A. Davó-Quiñonero, D. Lozano-Castello, A. Bueno-López, Sponge-like carbon monoliths: porosity control of 3D-printed carbon supports and its influence on the catalytic performance, Chem. Eng. J. 432 (2022) 134218.
[29] S. Hajimirzaee, A.M. Doyle, 3D printed catalytic converters with enhanced activity for low-temperature methane oxidation in dual-fuel engines, Fuel 274 (2020) 117848.
[30] S. Zakeri, T. Vastamäki, M. Honkanen, M. Järveläinen, M. Vippola, E. Levänen, Fabrication of self-supporting structures made of washcoat materials (γ-Al_2O_3-CeO_2) by ceramic stereolithography: towards digital manufacturing of enhanced catalytic converters, Mater. Des. 210 (2021) 110115.
[31] A. Tarancón, V. Esposito, M. Torrell, M. Di Vece, J.S. Son, P. Norby, D.B. Pedersen, 2022 roadmap on 3D printing for energy, J. Phys. Energy 4 (1) (2022) 011501.
[32] N. Kostretsova, A. Pesce, S. Anelli, M. Nuñez, A. Morata, F. Smeacetto, M. Torrell, A. Tarancón, Single-step fully 3D printed and co-sintered solid oxide fuel cells, J. Mater. Chem. A 12 (34) (2024) 22960–22970.
[33] M. Lira, N. Kostretsova, I. Babeli, L. Bernadet, S. Marquez, A. Morata, M. Torrell, Large-area 3D printed electrolyte-supported reversible solid oxide cells, Electrochim. Acta 467 (2023) 143074.
[34] A. Pesce, A. Hornés, M. Núñez, A. Morata, M. Torrell, A. Tarancón, 3D printing the next generation of enhanced solid oxide fuel and electrolysis cells, J. Mater. Chem. A 8 (2020) 16926.
[35] T.A. Le, M.S. Kim, S.H. Lee, T.W. Kim, E.D. Park, CO and CO_2 methanation over supported Ni catalysts, Catal. Today 293–294 (2017) 89–96.
[36] X. Liang, M. Wei, D. Dong, L. Lan, G. Yan, X. Yan, M. Liu, Applied research on methane steam reforming properties of porous structural catalyst fabricated by selective laser melting technology, Mater. Res. Express 11 (1) (2024) 016521.
[37] M. García-Vázquez, P. Marín, S. Ordóñez, K. Li, J. Tan, G. Zhang, F.R. García-García, Scaling up a hollow fibre reactor: a study on non-PGM hollow fibre after-treatments for methane emission control under extreme conditions, J. Environ. Chem. Eng. 9 (6) (2021) 106880.
[38] N. Kovacev, S. Li, S. Zeraati-Rezaei, H. Hemida, A. Tsolakis, K. Essa, Effects of the internal structures of monolith ceramic substrates on thermal and hydraulic properties: additive manufacturing, numerical modelling and experimental testing, Int. J. Adv. Manuf. Technol. 112 (2021) 1115–1132.
[39] T.H. Shih, W.W. Liou, A. Shabbir, Z. Yang, J. Zhu, A new k-ϵ eddy viscosity model for high reynolds number turbulent flows, Comput. Fluids 24 (3) (1995) 227–238.
[40] ANSYS FLUENT User's Guide 12.0. Using Flow Boundary Conditions. 2009
[41] Y. Wu, Y. Xu, S. Li, L. Zhong, J. Wang, Y. Chen, High-surface-area mesoporous silica-yttria-zirconia ceramic materials prepared by coprecipitation method–the role of silicon, Ceram. Int. 48 (15) (2022) 21951–21960.
[42] S. Tada, T. Shimizu, H. Kameyama, T. Haneda, R. Kikuchi, Ni/CeO2 catalysts with high CO_2 methanation activity and high CH4 selectivity at low temperatures, Int. J. Hydrog. Energy 37 (7) (2012) 5527–5531.
[43] E. Martín Morales, A. Alarcón, M. Biset-Peiró, E. Xuriguera, J. Guilera, Shaping of porous CeO2 powders into highly active catalyst carriers, ACS Appl. Eng. Mater. 1 (4) (2023) 1106–1115.
[44] S. Ratchahat, M. Sudoh, Y. Suzuki, W. Kawasaki, R. Watanabe, C. Fukuhara, Development of a powerful CO_2 methanation process using a structured Ni/CeO2 catalyst, J. CO_2 Util. 24 (July 2017) (2018) 210–219.
[45] G. Garbarino, D. Bellotti, P. Riani, L. Magistri, G. Busca, Methanation of carbon dioxide on Ru/Al2O3 and Ni/Al2O3 catalysts at atmospheric pressure: catalysts activation, behaviour and stability, Int. J. Hydrog. Energy 40 (30) (2015) 9171–9182.
[46] A. Vita, C. Italiano, L. Pino, P. Frontera, M. Ferraro, V. Antonucci, Activity and stability of powder and monolith-coated Ni/GDC catalysts for CO_2 methanation, Appl. Catal. B Environ. 226 (October 2017) (2018) 384–395.
[47] N. García-Moncada, J.C. Navarro, J.A. Odriozola, L. Lefferts, J.A. Faria, Enhanced catalytic activity and stability of nanoshaped Ni/CeO2 for CO_2 methanation in micro-monoliths, Catal. Today 383 (February 2021) (2022) 205–215.
[48] H.L. Huynh, W.M. Tucho, Q. Shen, Z. Yu, Bed packing configuration and hot-spot utilization for low-temperature CO_2 methanation on monolithic reactor, Chem. Eng. J. 428 (May 2021) (2021) 131106.

[49] J.C. Navarro, M.A. Centeno, O.H. Laguna, J.A. Odriozola, Ru–Ni/$MgAl_2O_4$ structured catalyst for CO_2 methanation, Renew. Energy 161 (2020) 120–132.
[50] C.Y. Chaparro-Garnica, P. Jordá-Faus, E. Bailón-García, R. Ocampo-Pérez, C. G. Aguilar-Madera, A. Davó-Quiñonero, D. Lozano-Castelló, A. Bueno-López, Customizable heterogeneous catalysts: nonchanneled advanced monolithic supports manufactured by 3D-printing for improved active phase coating performance, ACS Appl. Mater. Interfaces 12 (49) (2020) 54573–54584.
[51] O.P. Klenov, N.A. Chumakova, S.A. Pokrovskaya, A.S. Noskov, Impact of heat and mass transfer in porous catalytic monolith: CFD modeling of exothermic reaction, Chem. Eng. Sci. 205 (2019) 1–13.
[52] A. Quintanilla, G. Vega, P. Lopez, F. Garcia, E. Madurga, M. Belmonte, J.A. Casas, Enhanced fluid dynamics in 3D monolithic reactors to improve the chemical performance: experimental and numerical investigation, Ind. Eng. Chem. Res. 60 (41) (2021) 14701–14712.
[53] G. Vega, A. Quintanilla, N. Menendez, M. Belmonte, J.A. Casas, 3D honeycomb monoliths with interconnected channels for the sustainable production of dihydroxybenzenes: towards the intensification of selective oxidation processes, Chem. Eng. Process. - Process. Intensif. 165 (December 2020) (2021).
[54] S. Renda, A. Ricca, V. Palma, Insights in the application of highly conductive structured catalysts to CO_2 methanation: computational study, Int. J. Hydrog. Energy 48 (96) (2023) 37473–37488.
[55] A. Ricca, L. Truda, V. Palma, Study of the role of chemical support and structured carrier on the CO2 methanation reaction, Chem. Eng. J. 377 (ember 2018) (2019) 120461.
[56] A. Parra-Marfil, R. Ocampo-Pérez, C.G. Aguilar-Madera, F. Carrasco-Marín, A. F. Pérez-Cadenas, A. Bueno-López, E. Bailón-García, Modeling and experimental analysis of CO2 methanation reaction using Ni/CeO2 monolithic catalyst, Environ. Sci. Pollut. Res. (0123456789) (2024).